

Interaction Phenomena at Reactive Metal/Ceramic Interfaces¹

S. M. McDeavitt, G.W. Billings* and J.E. Indacochea**

Argonne National Laboratory, Argonne, IL

**Integrated Thermal Sciences, Inc., Santa Rosa, CA*

***University of Illinois at Chicago, Chicago, IL*

To be Published in the Proceedings of the
International Conference on Joining of Advanced and Specialty Materials III
ASM International
St. Louis, MO, October 9-12, 2000

The submitted manuscript has been created by the University of Chicago as Operator of Argonne National Laboratory ("Argonne") under Contract No. W-31-109-ENG-38 with the U.S. Department of Energy. The U.S. Government retains for itself, and others acting on its behalf, a paid-up, nonexclusive, irrevocable worldwide license in said article to reproduce, prepare derivative works, distribute copies to the public, and perform publicly and display publicly, by or on behalf of the Government.

¹Work supported by the U.S. Department of Energy, Nuclear Energy Research & Development Program, under Contract W-31-109-Eng-38

DISCLAIMER

This report was prepared as an account of work sponsored by an agency of the United States Government. Neither the United States Government nor any agency thereof, nor any of their employees, make any warranty, express or implied, or assumes any legal liability or responsibility for the accuracy, completeness, or usefulness of any information, apparatus, product, or process disclosed, or represents that its use would not infringe privately owned rights. Reference herein to any specific commercial product, process, or service by trade name, trademark, manufacturer, or otherwise does not necessarily constitute or imply its endorsement, recommendation, or favoring by the United States Government or any agency thereof. The views and opinions of authors expressed herein do not necessarily state or reflect those of the United States Government or any agency thereof.

DISCLAIMER

Portions of this document may be illegible in electronic image products. Images are produced from the best available original document.

Interaction Phenomena at Reactive Metal/Ceramic Interfaces

S. M. McDevitt, G.W. Billings & J.E. Indacochea[†]*

Argonne National Laboratory, Argonne, IL

**Integrated Thermal Sciences, Inc., Santa Rosa, CA*

[†]University of Illinois at Chicago, Chicago, IL

Presented at ASM Materials Solutions

October 9, 2000 St. Louis, MO

RECEIVED

DEC 08 2000

OSTI

Abstract

The objective of this study was to understand the interface chemical reactions between stable ceramics and reactive liquid metals, and developing microstructures. Experiments were conducted at elevated temperatures where small metal samples of Zr and Zr-alloy were placed on top of selected oxide and non-oxide ceramic substrates (Y_2O_3 , ZrN, ZrC, and HfC). The sample stage was heated in high-purity argon to about 2000°C, held in most cases for five minutes at the peak temperature, and then cooled to room temperature at $\sim 20^\circ\text{C}/\text{min}$. An external video camera was used to monitor the in-situ wetting and interface reactions. Post-test examinations of the systems were conducted by scanning electron microscopy and energy dispersive spectroscopy. It was determined that the Zr and the Zr-alloy are very active in the wetting of stable ceramics at elevated temperatures. In addition, in some systems, such as Zr/ZrN, a reactive transition phase formed between the ceramic and the metal. In other systems, such as Zr/ Y_2O_3 , Zr/ZrC and Zr/HfC, no reaction products formed, but a continuous and strong joint developed under these circumstances also.

Introduction

Ceramic-metal interfaces are important in several technologies, where the interfacial morphology may control the performance characteristics of dissimilar

material joints, metal-matrix composites, electronic packages, glass-to-metal seals, and liquid metal process systems.

Microstructure development at ceramic-metal interfaces plays a key role in all the processes mentioned above. Joining and composite processing procedures require the formation of continuous interfaces with good mechanical strength and toughness to withstand process-induced or service-induced stresses. In ceramic joining, a metal interlayer provides a transition region across two brittle and often dissimilar materials.

There are applications where wetting and formation of a ceramic-metal interface are not desired. In metal casting, for example, a refractory crucible is used to contain the liquid metal, and ceramic porous bodies are used as filter materials.

In both joining and composite fabrication, continuous interfaces can be achieved in the solid state by hot isostatic pressing or by a liquid state process through wetting and spreading of a liquid metal on a ceramic surface. Furthermore, nearly all ceramic-metal couples exhibit a large coefficient of thermal expansion mismatch, which leads to the development of large thermal stresses during cooling from processing [1, 2] or from thermal cycling in service. In general, these stresses must be relieved by the plastic deformation of the metallic phase, or cracks can develop at the ceramic-metal interface or

in the ceramic near the interface [3-5]. Ideally, a ductile metal (e.g., copper or aluminum) can be used to deform and relieve these thermal stresses. However, most ductile metals do not wet ceramics.

The basic cause of ceramic non-wettability is the unusually nonmetallic, ionic or covalent, bonding of their lattices and consequent lack of delocalized binding electrons needed to continue a metallic condition and hence create a low energy ceramic-metal interface. The energy of such an interface is usually larger than that of the ceramic substrate. Wetting is reckoned to be acceptable if the contact angle (Figure 1) is less than 90° and preferably less than 20° for a successful braze. To achieve the necessary decrease in γ_{SL} , the chemistry of the interface must be changed, and the addition of a reactive metal results in the reduction of the ceramic phase and formation of new phases at the ceramic-metal interface [6-9]. Reaction product sequences can become complex, and the resulting structure is often an elaborate series of interfacial product layers. The thickness and mechanical properties of each phase, the coefficient of thermal expansion mismatch, and adhesion at each interface, all play a role in the final properties of the joint or composite structures [4, 7].

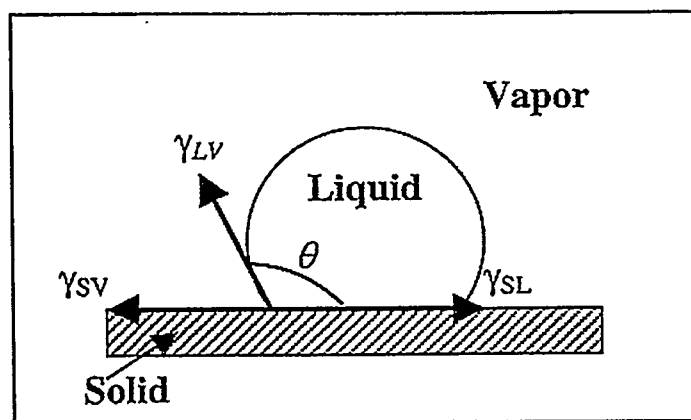


Figure 1. Sessile drop configuration showing the contact angle for a non-wetting condition ($\theta > 90^\circ$).

The work presented in this article considers the reactions at the ceramic-metal interface and the microstructures that develop during melting and exposures to high temperatures. The results of the interactions of yttria, zirconium-nitride, zirconium-

carbide, and hafnium-carbide with zirconium metal and zirconium metal alloys are given here.

Materials and Experimental Procedure

High-temperature experiments were conducted by placing small metal samples onto ceramic substrates. A wide variety of oxides and other ceramics were fabricated from high purity powders by hot uniaxial pressing (HUP). All materials were cleaned prior to the tests, using acetone to remove dirt and other contaminants from the materials. The metal specimens included pure Zr, Zr + 8 wt. % ferritic stainless steel, and ferritic stainless steel alloyed with 15 wt. % Zr. The composition of the stainless steel (HT-9) in weight percent is 0.5Ni, 12.0Cr, 0.2Mn, 1.0Mo, 0.25Si, 0.5W, 0.5V, 0.2C, and balance Fe. The metal/ceramic combination was heated in a tungsten mesh furnace in high purity argon with a sensing thermocouple placed about 0.5 cm beneath the samples. The materials were preheated to 600°C , continuously heated at a rate of about $20^\circ\text{C}/\text{min}$ to 1600°C , and then at $10^\circ\text{C}/\text{min}$ to 2000°C . In most cases, the peak temperature was held for 5 min and then cooled at $\sim 20^\circ\text{C}/\text{min}$.

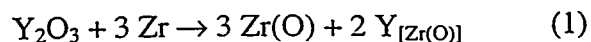
The wetting and high temperature interactions between the molten metals and ceramic substrates were monitored through an external video camera. In-situ observations were followed by post-test examinations using scanning electron microscopy (SEM) and energy dispersive spectroscopy (EDS).

Results and Discussion

Zr - Y_2O_3 System

No reactions were observed at the interface before melting of zirconium. Melting occurred at $\sim 1850^\circ\text{C}$, and the molten Zr immediately wetted the Y_2O_3 (Figure 1); a contact angle of $\sim 50^\circ$ was measured.

Interfacial reactions occurred, as confirmed by the liquid bubbling at the interface, observed in the video. There were microstructural changes at the interface and in the Zr metal. The likely chemical reaction is reduction of the Y_2O_3 by Zr metal described by:



ZrO₂ is unlikely to form in this reaction since Y₂O₃ is more stable from equilibrium thermodynamics. Thus, both O and Y are expected to dissolve in molten Zr. Figures 2 and 3 show evidence of such dissolution. Right at the Zr-Y₂O₃ interface a light reaction band, ~25 μm thick, was observed. Furthermore, some black precipitate decorates the grain boundaries of the Zr metal. Both of these features are better observed in Figure 3. EDS analysis showed that oxygen dissolved in Zr metal, the light band at the interface was rich in oxygen, and Y segregated to the grain boundaries. The Y segregation is caused by a lower solubility of this element in α-Zr. The oxygen enrichment of the Zr at the interface is likely caused by the proximity to the oxide ceramic, where the localized chemical reduction was occurring.

The interface was rugged as a result of the chemical reaction, as seen in Figure 3. The ceramic surface was polished prior to the sessile experiment. But no transition phase developed at this location as a result of the localized chemical reaction. Yet continuity existed across the interface, and the solidified metal droplet was tightly bonded to the ceramic substrate.

Stainless Steel / 15wt. % Zr - Y₂O₃ System

The eutectic melting point of the alloy stainless steel is ~1530°C, and as expected the metal piece melted at this temperature and in a way masked any possible reaction between the metal alloy, particularly Zr, and the Y₂O₃ substrate. Nonetheless, the liquid metal did not wet the ceramic immediately following melting. The contact angle was measured initially at ~110°, and it varied unexpectedly with increasing temperature. It dropped to 95° at 1370°C, but it increased again to ~140° as the temperature reached 1950°C. When the temperature approached ~2000°C the contact angle was reduced to 90°, and finally to 60° as the system was held at the peak temperature for 5 minutes before cooling.

The metal droplet bonded to the Y₂O₃, but it separated on cooling because of the differences in the coefficients of thermal expansion. Extensive cracking was found in the ceramic substrate adjacent to the interface (Figure 4).

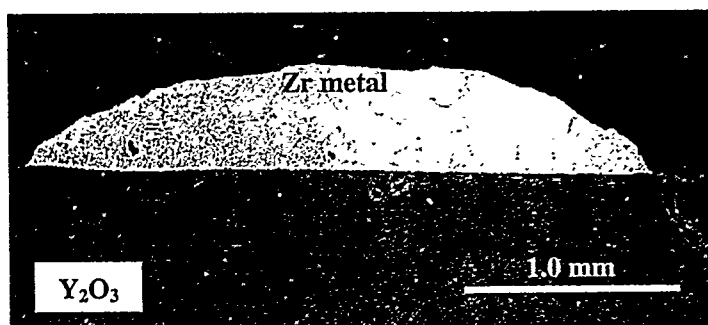


Figure 2. Wetting of the Y₂O₃ by the molten Zr.

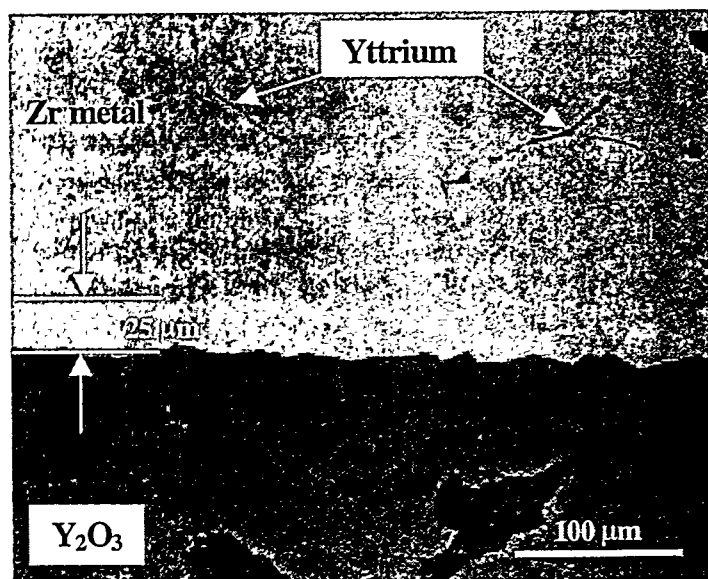


Figure 3. Microstructural features in Zr-Y₂O₃ system. Oxygen-rich reaction band at the interface and grain boundaries rich with yttrium.

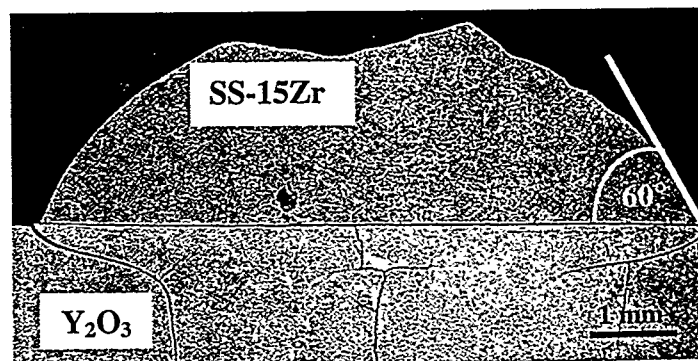


Figure 4. SS-15Zr alloy and Y₂O₃ interface. Metal alloy separated from the substrate, and cracking is seen in the substrate.

This system showed an yttrium-rich transition reaction layer between the metal alloy and the ceramic substrate, as seen in Figure 5. The reaction

layer was very thin and not uniform in thickness, which may explain why the metal separated from the ceramic easily. The formation of this transition layer was unlike what was observed in the pure Zr metal where no distinct layer was perceived.

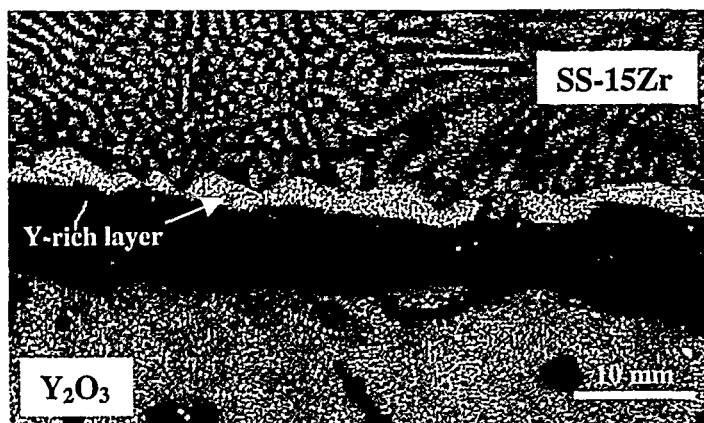


Figure 5. Reaction layer at the interface between the SS-15Zr alloy and Y_2O_3 .

Zr / 8wt. % Stainless Steel – Y_2O_3 System

Chemical reactions at the interface were observed in this system, similar to the behavior of Zr/ Y_2O_3 . Bubbling was seen at the liquid-ceramic interface at $\sim 1850^\circ C$, and at $\sim 1870^\circ$ the metal alloy melted entirely and wetted the Y_2O_3 ($\theta = 35^\circ-40^\circ$). The reaction thickness at the interface was between 10 and 20 μm .

Oxygen from the interface reaction was observed from wavelength dispersion spectroscopy (WDS) to have dissolved in the metal droplet, but yttrium was not detected in the metal and primarily stayed at the reaction zone instead. Results of this chemical analysis are shown in Figure 6.

In this system there was again a smooth transition between the metal droplet and the ceramic substrate. No distinct reaction layer was formed, although a light reaction region was observed. The metal alloy was strongly bonded to the Y_2O_3 , and no cracking was visible.

Zr / ZrN System

The Zr did not begin melting at the interface with ZrN until $\sim 1975^\circ C$. This increase in the melting point of Zr can only be attributed to the diffusion of

nitrogen into the pure Zr before melting. This indicates then that a chemical reaction at the interface between the Zr metal and the ZrN must have occurred before melting. According to the equilibrium phase diagram of Zr and N [10], β -Zr has a maximum solubility of 0.8 wt. % nitrogen. This composition should melt at $\sim 1880^\circ C$. When the N content in Zr is between 3 and 5 wt. %, the alloy is α -Zr, and the melting temperature ranges between $\sim 1880^\circ C$ and $\sim 1985^\circ C$, respectively. The Zr metal melted fully at $\sim 2000^\circ C$ and wetted the ZrN.

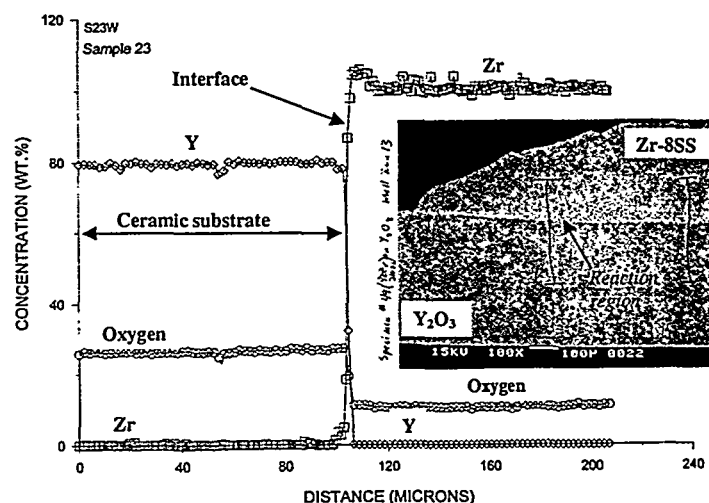


Figure 6. WDS analysis from substrate, across the interface into the metal drop in Zr-8SS/ Y_2O_3 .

A microstructural analysis of the system after the thermal test shows a distinct reaction layer, about 70 to 90 μm thick, at the interface between the solid metal alloy and the ZrN (Figure 7). A continuous crack was observed that ran along the reaction band at the metal side. This crack is due to the differences in the coefficients of thermal expansion. No other cracks were found in either of the two materials.

The reaction layer is composed of a newly precipitated ZrN band, about 35 to 45 μm , at the metal droplet side; and a similar-size reaction region is found in the ceramic substrate, light gray. Figure 8 shows more clearly the reaction zone. The interface between the newly formed ZrN and the reacted ZrN region of the substrate was smooth and uniform, and there was no infiltration of pure Zr metal into the substrate. Except for the long crack at the interface, the Zr/ZrN joint appeared quite strong. In addition to

the precipitation of new ZrN at the interface, Zr lath-like precipitates were observed throughout the solidified metal droplet resting on top of the ZrN substrate (Figures 7 and 8).

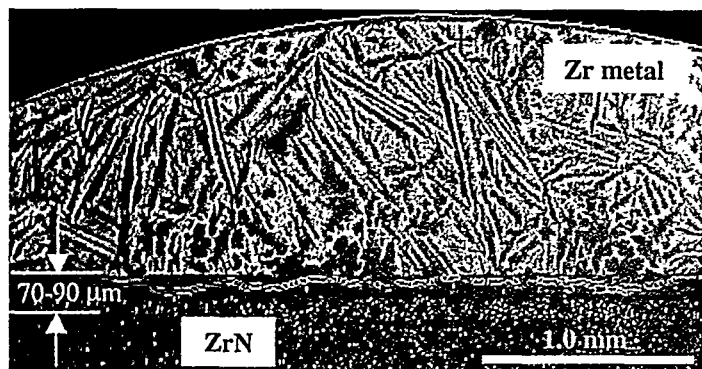


Figure 7. Microstructure changes from the interaction between pure Zr metal and ZrN substrate.

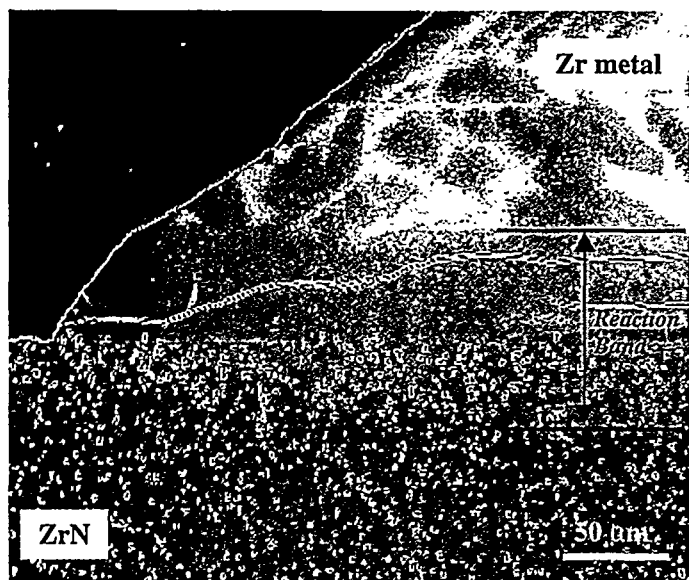


Figure 8. SEM micrograph depicting the reaction band in the Zr/ZrN system.

Zr / ZrC System

The Zr metal melted completely by $\sim 1910^{\circ}\text{C}$, and no chemical reactions were detected in the video before melting. Furthermore, following melting the molten Zr flowed readily over the ZrC surface and spilled over to the sides of the ZrC specimen. The liquid metal finally rested on the tungsten dish that held the ZrC substrate. It also penetrated in between

the tungsten holder and the ZrC, and bonded these two materials together (Figure 9).

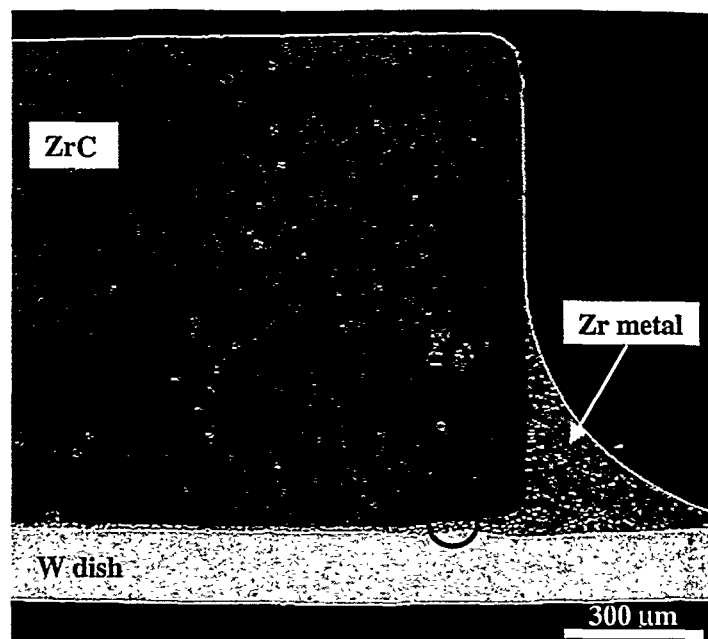


Figure 9. The pure molten Zr metal flowed easily over the ZrC and brazed the ZrC to the W metal holder.

The top surface of the ZrC was clean and smooth, with no sign of a possible chemical reaction between the Zr metal and the ZrC. There was a lack of chemical reaction of this system in contrast to that of the ZrN substrate. From standard thermodynamics data, the stability of the ZrN is greater than that of ZrC up to temperatures of about 1200°C . However, the rate of decrease in stability with temperature is faster for ZrN than for ZrC. Review of the Zr-C equilibrium binary phase diagram (Figure 10) shows that both $\alpha\text{-Zr}$ and $\beta\text{-Zr}$ have limited solubility for carbon, but either phase is in equilibrium with ZrC.

The braze joint between the ZrC substrate and the W metal holder was metallographically analyzed. This was done to establish the extent of the Zr/ZrC interaction at the bottom of the ZrC. There was a strong bonding at the interface of the W and the ZrC. Also no cracking was observed in either material or in the Zr braze metal. Figure 11 gives more detail of the ZrC-W joint, which corresponds to the circle in Figure 9. The interface between the $\alpha\text{-Zr}$ and the ZrC is smooth, and it does not show any form of degradation or extensive chemical reaction. The

microstructure at this Zr/ZrC interface complies with what is presented in the equilibrium phase diagram (Figure 10). On the opposite side of the braze metal, the molten Zr reacted with W. According to the Zr-W equilibrium phase diagram [12], there is a eutectic at Zr - 16.6 wt. % W with a melting temperature of about 1735°C. The microstructure encountered in the joint agrees with what is described in the phase diagram. That is, the braze metal consists of a matrix of α -Zr with a eutectic consisting of W_2Zr intermetallic; closer to the W metal there is a layer of the same W_2Zr intermetallic attached to the base metal. An EDS analysis of the intermetallic particles confirmed their composition.

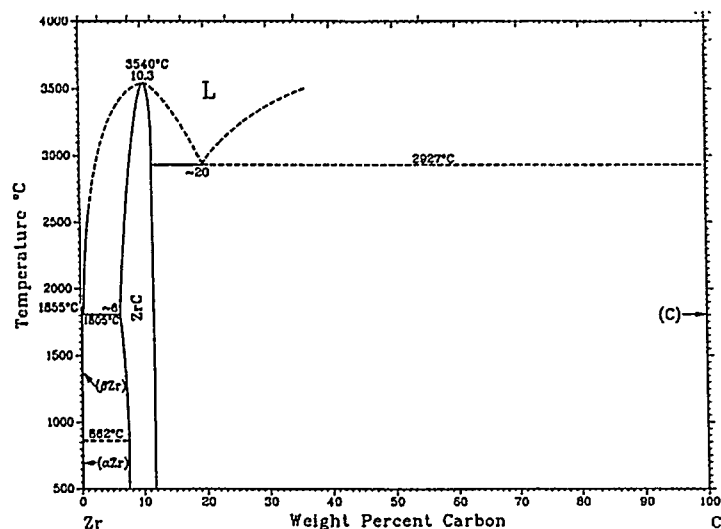


Figure 10. Equilibrium binary phase diagram of Zr and C [11].

Zr / HfC System

This system behaved similarly to that of the Zr/ZrC. Zirconium melted completely at ~1915°C and also flowed freely, but this time the melt was confined to the top of the HfC surface. No chemical reactions were observed prior to melting. The fact that the solidified Zr metal remained well bonded to the HfC substrate suggests some interface interaction between these two materials. There was no transition reaction layer in this system either, as seen in Figure 12.

The possibility of limited interface reduction of the HfC cannot be ruled out since there was a slight increase in the melting temperature of the Zr.

According to the equilibrium phase diagram (Figure 13), Hf will increase the liquidus temperature of a Zr-Hf alloy.

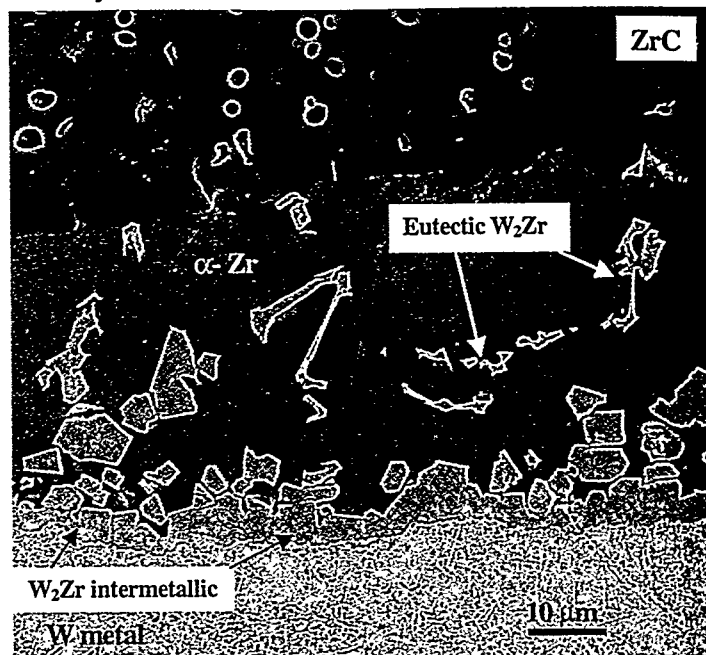


Figure 11. ZrC joined to the tungsten metal via Zr-metal.

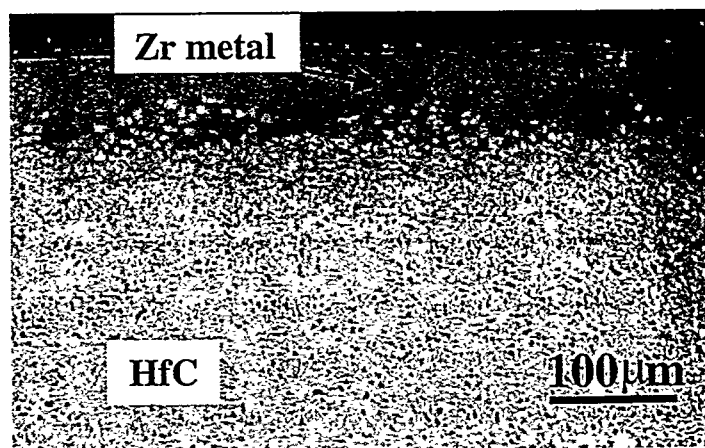


Figure 12. Pure Zr metal flow on top of HfC and interface interactions between the two materials.

Another indication of dissolution or chemical reaction between hafnium carbide and the zirconium melt is the partial degradation of the surface of the HfC substrate. This is observed in Figure 12, where some grains of HfC have pulled away from the ceramic substrate. In the same micrograph some of these grains are seen to have floated into the zirconium melt.

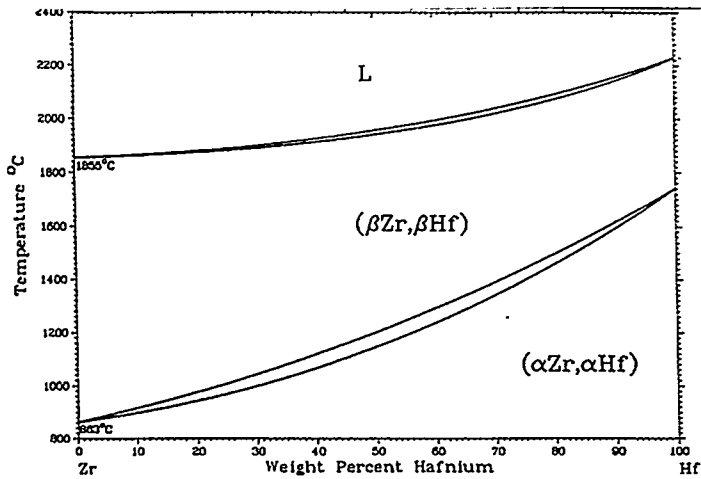


Figure 13. Equilibrium phase diagram of Zr and Hf [13].

Conclusions

1. Zirconium and zirconium alloys stimulate reactive wetting of stable ceramics at high temperatures.
2. Chemical reactivity and impurity solubility play significant roles in the wetting mechanics.
3. Conventional reaction products were observed at the SS-15Zr/Y₂O₃, Zr/ZrN and Zr/W interfaces.
4. No reaction products were observed across the Zr/Y₂O₃, Zr/ZrC, and Zr/HfC interfaces, but a continuous and strong bond developed.

References

1. Y.L. Shen, J. Mater. Sci. Eng., Vol. A252, pp. 269-275 (1998).
2. S.P. Kovalev, P. Miranzo, and M.I. Osendi, J. Amer. Ceram. Soc., Vol. 81, pp. 2342-2348 (1998).
3. F. Hatakeyama, K. Suganuma, and T. Okamoto, J. Mat. Sci., Vol. 21, pp. 2455-2461 (1986).
4. A. Bartlet, A.G. Evans, and M. Ruhle, Acta Met., Vol. 39, pp. 1579-1585 (1991).
5. A.G. Evans and B.G. Dalgleisch, J. Mater. Sci. Eng., Vol. A162, pp. 1-13 (1993).

6. A.J Moorhead and H. Keating, Weld J., Vol. 65, pp. 17-31 (1986).
7. L. Espie, B. Drevet, and N. Eustathopoulos, Met. Trans A, Vol. 25A, pp. 599-605 (1994).
8. P. Kristalis et al., Scripta Met., Vol. 30, pp. 1127-1132 (1994).
9. P. Xiao and B. Derby, Acta Mat., Vol. 46, pp. 3491-3499 (1998).
10. Binary Alloy Phase Diagrams, Second Edition, Vol. 3, p. 2717, ASM International (1990).
11. Binary Alloy Phase Diagrams, Second Edition, Vol. 1, p. 900, ASM International (1990).
12. Binary Alloy Phase Diagrams, Second Edition, Vol. 3, p. 3534, ASM International (1990).
13. Binary Alloy Phase Diagrams, Second Edition, Vol. 3, p. 2129, ASM International (1990).